



**HAL**  
open science

## Synaptic communication mediates the assembly of a self-organizing circuit that controls reproduction

Matan Golan, J. Boulanger-Weill, A. Pinot, Pierre Fontanaud, Adèle Faucherre, D. Gajbhiye, L. Hollander-Cohen, T. Fiordelasio-Coll, Agnès O Martin, Patrice Mollard

### ► To cite this version:

Matan Golan, J. Boulanger-Weill, A. Pinot, Pierre Fontanaud, Adèle Faucherre, et al.. Synaptic communication mediates the assembly of a self-organizing circuit that controls reproduction. *Science Advances*, 2021, 7 (8), pp.eabc8475. 10.1126/sciadv.abc8475. hal-03151096

**HAL Id: hal-03151096**

**<https://hal.science/hal-03151096>**

Submitted on 31 May 2021

**HAL** is a multi-disciplinary open access archive for the deposit and dissemination of scientific research documents, whether they are published or not. The documents may come from teaching and research institutions in France or abroad, or from public or private research centers.

L'archive ouverte pluridisciplinaire **HAL**, est destinée au dépôt et à la diffusion de documents scientifiques de niveau recherche, publiés ou non, émanant des établissements d'enseignement et de recherche français ou étrangers, des laboratoires publics ou privés.



Distributed under a Creative Commons Attribution - NonCommercial 4.0 International License

## NEUROSCIENCE

# Synaptic communication mediates the assembly of a self-organizing circuit that controls reproduction

M. Golan<sup>1,2\*</sup>, J. Boulanger-Weill<sup>3</sup>, A. Pinot<sup>4</sup>, P. Fontanaud<sup>1,4</sup>, A. Faucherre<sup>1</sup>, D. S. Gajbhiye<sup>2</sup>, L. Hollander-Cohen<sup>5</sup>, T. Fiordelisio-Coll<sup>1,6</sup>, A. O. Martin<sup>1</sup>, P. Mollard<sup>1,4\*</sup>

Migration of gonadotropin-releasing hormone (GnRH) neurons from their birthplace in the nasal placode to their hypothalamic destination is critical for vertebrate reproduction and species persistence. While their migration mode as individual GnRH neurons has been extensively studied, the role of GnRH-GnRH cell communication during migration remains largely unexplored. Here, we show in awake zebrafish larvae that migrating GnRH neurons pause at the nasal-forebrain junction and form clusters that act as interhemisphere neuronal ensembles. Within the ensembles, GnRH neurons create an isolated, spontaneously active circuit that is internally wired through monosynaptic glutamatergic synapses into which newborn GnRH neurons integrate before entering the brain. This initial phase of integration drives a phenotypic switch, which is essential for GnRH neurons to properly migrate toward their hypothalamic destination. Together, these experiments reveal a critical step for reproduction, which depends on synaptic communication between migrating GnRH neurons.

## INTRODUCTION

Neuronal migration is a critical process for brain development and function. One key example is the migration of the small population of gonadotropin-releasing hormone (GnRH) neurons, which are born in the nasal placode (NP) and migrate during embryonic development along the tract of the terminal nerve into their final location in the hypothalamus (1), a process that is conserved across all vertebrates (2). Since GnRH neurons are master regulators of reproduction (3), defects in their migration lead to reproductive dysfunction and infertility, as observed in human patients with Kallmann syndrome (1, 2). Correct guidance of GnRH neuron migration from the NP toward their final brain location is therefore critical for the propagation of the species.

During their initial stage of migration, GnRH neurons pause and form tight clusters at the cribriform plate, located at the boundary between the NP and brain. This pause has been observed in avians (4), rodents (5), and humans (6), yet its role and underlying processes remain unknown. A transitory pause and aggregation have also been reported in other migratory neuron populations at the interface between two extracellular environments (7–9). In neocortical and hippocampal migrating neurons, the pause has been shown to precede a phenotypic switch of the cell shape, speed, and mode of migration (7, 8) and is therefore considered a key stage that is required for the transition into a new environment. However, the factors that cause the cells to halt and drive the phenotypic switch remain poorly understood.

Among the signaling processes critical for neuronal migration, neuronal activity plays an important role (10, 11), in part, through downstream modulation of calcium concentrations (12, 13) that induce rearrangement of cytoskeletal elements (14). In addition to its direct role in the control of motility, neuronal activity also modulates gene expression (15, 16), thus providing a pathway by which external inputs can shape the molecular signature and hence the phenotype of neurons. Increased neuronal activity has been shown to induce transcriptional changes that act as a stop signal and lead to precocious maturation of migrating neurons (17, 18). The pause and compact organization of GnRH neurons at the nasal-forebrain junction (NFJ) prompted us to hypothesize that cell-cell communication during the pause modulates GnRH neuronal activity, thus orchestrating a transition that allows GnRH cells to cross the cribriform plate and make their way into the brain.

We therefore studied the behavior of GnRH neurons to gain insight into the processes that take place during the pause at the entrance to the brain. By using zebrafish as a vertebrate model, we performed longitudinal *in vivo* imaging studies of the migration of GnRH neurons in awake fish larvae along with real-time monitoring of spontaneous calcium dynamics due to GnRH3 neuron excitability within their natural niche. We found that when NP-originating GnRH neurons locally colonize the brain border, they enter a 3-day pause in which they form an isolated circuit and interact via *N*-methyl-D-aspartate (NMDA)-activated glutamatergic synapses within two GnRH clusters, which are interconnected between both hemispheres. Coordinated GnRH neuron activity initially emerges from their synaptic connectivity. Following the pause, GnRH neurons undergo a marked morphological transition as they enter the brain. By manipulating their connectivity and activity, we show that establishment of a circuit-intrinsic process is critical for the ability of GnRH neurons to enter the brain toward their functional hypothalamic target.

## RESULTS

In zebrafish, terminal nerve (TN) GnRH3 neurons are considered homologous to the hypophysiotropic GnRH1 neurons found in

Copyright © 2021  
The Authors, some  
rights reserved;  
exclusive licensee  
American Association  
for the Advancement  
of Science. No claim to  
original U.S. Government  
Works. Distributed  
under a Creative  
Commons Attribution  
NonCommercial  
License 4.0 (CC BY-NC).

<sup>1</sup>Institute of Functional Genomics, University of Montpellier, CNRS, INSERM, France.

<sup>2</sup>Institute of Animal Science, Agricultural Research Organization, P.O. Box 15159, Rishon Letzayon, 7505101, Israel. <sup>3</sup>Department of Molecular and Cellular Biology, Center for Brain Science, Harvard University, Cambridge, MA, USA. <sup>4</sup>BioCampus Montpellier, University of Montpellier, CNRS, INSERM, F-34094 Montpellier, France.

<sup>5</sup>Department of Animal Sciences, The Robert H. Smith Faculty of Agriculture, Food, and Environment, The Hebrew University of Jerusalem, Rehovot 76100, Israel.

<sup>6</sup>Laboratorio de Neuroendocrinología Comparada, Departamento de Ecología y Recursos Naturales, Biología, Facultad de Ciencias, Universidad Nacional Autónoma de México, Ciudad Universitaria, 04510 México, DF, México.

\*Corresponding author. Email: matan.golan@mail.huji.ac.il (M.G.) patrice.mollard@igf.cnrs.fr (P.M.)

other vertebrates due to their birthplace in the NP (19), their migratory nature (20), and their hypophysiotropic projections (21). Functional homology is supported by the fact that GnRH3 neurons are key regulators of reproduction in zebrafish as evidenced by the reproductive dysfunction caused by the specific loss of these cells during development (22) or in adulthood (fig. S1). We therefore targeted GnRH3-expressing cells by using the zebrafish GnRH3 promoter (20) to drive expression of foreign proteins specifically in GnRH3 neurons (fig. S2, A and B).

The embryonic origin of the hypophysiotropic GnRH neurons in zebrafish has been under debate (23). While some groups have pointed to a hypothalamic origin (24, 25), others have identified the migratory population of GnRH3 neurons that are born in the NP as the one projecting toward the pituitary and controlling reproduction (19, 20). Some of the uncertainty may stem from early GnRH3 expression in the hypothalamus where cell bodies are in close proximity to the pituitary, as can be observed in some transgenic lines (24). However, tracing the hypophysiotropic projections of GnRH3 neurons in the intact adult cleared brain (fig. S2, C to E) reveals that only the nasal-born, migratory GnRH3 subpopulations innervate the pituitary gland. Notably, it has been reported that GnRH3 knockout zebrafish remain fertile (26, 27). In these studies, GnRH3 knockout fish exhibited an increase of other reproductive neuropeptides in the brain that were thought to compensate for the loss of the GnRH3 peptide (28, 29). Ablation of GnRH3 neurons, either during development (22) or in adulthood (fig. S1), caused infertility in our fish experiments.

### Migrating GnRH3 neurons make a 3-day pause at the entrance to the brain and undergo a marked morphological transition

We first explored the real-time dynamics of GnRH3 neuronal migration in vivo. In zebrafish, GnRH3 neurons are born in the NP at approximately 24 hours after fertilization and migrate to the brain along the axons of the TN during the course of development (Fig. 1A, fig. S3, and movie S1). We categorized the migrating GnRH3 population, according to their position, into three stages (Fig. 1B): (i) Nasal GnRH cells are newborn neurons that are still located in the NP. These cells migrate toward the interface between the NP and the brain. Figure 1C (top) and movie S2 show an example of a migrating nasal GnRH cell. (ii) When GnRH3 cells reach the NFJ, they halt for several days and form a cluster-like aggregation. (iii) Brain GnRH cells have left the NFJ and entered the brain. Figure 1C (bottom) and movie S3 show an example of two migrating NFJ cells leaving the cluster. To follow the fate of the cells during several days, we expressed the photoconvertible protein Kaede in GnRH cells. Kaede can be converted from green to red using blue light (30). Photoconversion of kaede-expressing cells in the NFJ cluster at 3 days post fertilization (dpf) allowed us to follow their migration into the brain on subsequent days and provide further proof that brain GnRH cells originate from the NFJ cluster (fig. S4). Brain GnRH3 cells halt along their migration path, forming a continuum of cells from the NP to the hypothalamus (Fig. 1A), in a pattern that persists through to adulthood (fig. S2C and D). Starting at 3 dpf, the number of cells at the NFJ remains constant ( $16.5 \pm 1.6$  total NFJ cells,  $n = 8$ ), while the number of cells that have crossed into the brain steadily increases, suggesting a constant flow of newborn cells into the system. Because GnRH3 neurons are born in the NP at  $\sim 1$  dpf and first appear in the brain fraction at 4 dpf, we could establish that migrating GnRH neurons made an average pause of approximately

3 days at the NFJ before entering the brain (Fig. 1D), although we cannot rule out the possibility that some cells may have a longer or shorter residency at the NFJ. The existence of the NFJ cluster is transient and cannot be observed in mature fish (fig. S2C and D), indicating that most GnRH3 neurons (approximately 100 cells in the adult zebrafish) will finally make their way into the brain.

By measuring the morphometric parameters of cells in the different compartments, we noticed that GnRH3 cells undergo a marked morphological transition upon entering the brain. The transition is evident in brain GnRH cells that exhibit an elongated shape that is markedly different from the largely circular shape of nasal or NFJ cells (Fig. 1, E to G). This morphological change takes place as the cells leave the NFJ (movie S3) and is retained in almost all the cells that have entered the brain.

### Pausing GnRH3 cells form ensembles of co-active neurons

To study the behavior of GnRH3 neurons during their migration, we followed their spontaneous activity through in vivo calcium imaging. Using two-photon microscopy, we imaged calcium dynamics in awake fish that express the genetically encoded calcium indicator GCaMP6s or R-CaMP2 in GnRH3 neurons [Tg(GnRH3:gal4ff; UAS:GCaMP6s) or Tg(GnRH3:R-CaMP2), respectively]. Spontaneous calcium activity of GnRH3 neurons began at 2 dpf and was observed at least until 15 dpf (the latest stage tested in the current study). By combining in vivo calcium imaging and loose-patch recordings of NFJ GnRH3 neurons, we observed endogenous electrical events with each of them correlated with detectable calcium transients (Fig. 2A), suggesting that monitoring calcium signals could be used as a reporter of electrical activity as reported for mammalian GnRH neurons (31). Comparing the calcium profile of cells in the different categories, we found that spontaneous calcium activity was highly synchronized within the GnRH3 population of both NFJ and brain but not nasal GnRH cells (Fig. 2, B and C; fig. S5; and movies S4 to S6). The high intra- and interhemisphere coordination persisted at least until 8 dpf (fig. S6).

Unexpectedly, calcium transients were highly synchronized not only between the cells of the same hemisphere, but also, to a slightly lesser degree, between the two hemispheres (Fig. 2, B and E, and fig. S7A; intracluster correlation  $0.93 \pm 0.008$  and  $0.94 \pm 0.006$  in 3 and 6 dpf, respectively; intercluster correlation  $0.86 \pm 0.011$  and  $0.88 \pm 0.01$  in 3 and 6 dpf, respectively.  $n = 14$  3-dpf fish and 15 6-dpf fish).

We then compared the level of coordination of cells in different positions along the migration pathway to generate a complete correlation matrix of the GnRH3 circuit. While brain GnRH neurons were highly synchronized with cells at the NFJ both within and between hemispheres, most nasal GnRH cells showed both a low cell-cell coordination within the NP and to GnRH cells at the NFJ or in the brain (Fig. 2, B to E;  $n = 55$  nasal, 181 NFJ, and 31 brain GnRH neurons from 29 6-dpf fish. Also see fig. S5 and movies S4 to S6). In the cases where a nasal cell was coordinated with the NFJ cells ( $r > 0.5$ , 42.6% of cases), a neurite from the nasal cell could usually be observed projecting into the NFJ cluster (movie S7). Apart from their low level of coordination, nasal GnRH3 cells also exhibited a different calcium signature with slightly lower event frequency, a markedly lower amplitude and a decreased transient duration. In addition, 14% of nasal GnRH cells were silent ( $n = 55$  nasal, 181 NFJ, and 31 brain GnRH neurons from 29 6-dpf fish; Fig. 2, F to I, and fig. S7).

A morphological analysis of individual genetically labeled GnRH3 neurons (fig. S8) supports the existence of contralateral and ipsilateral

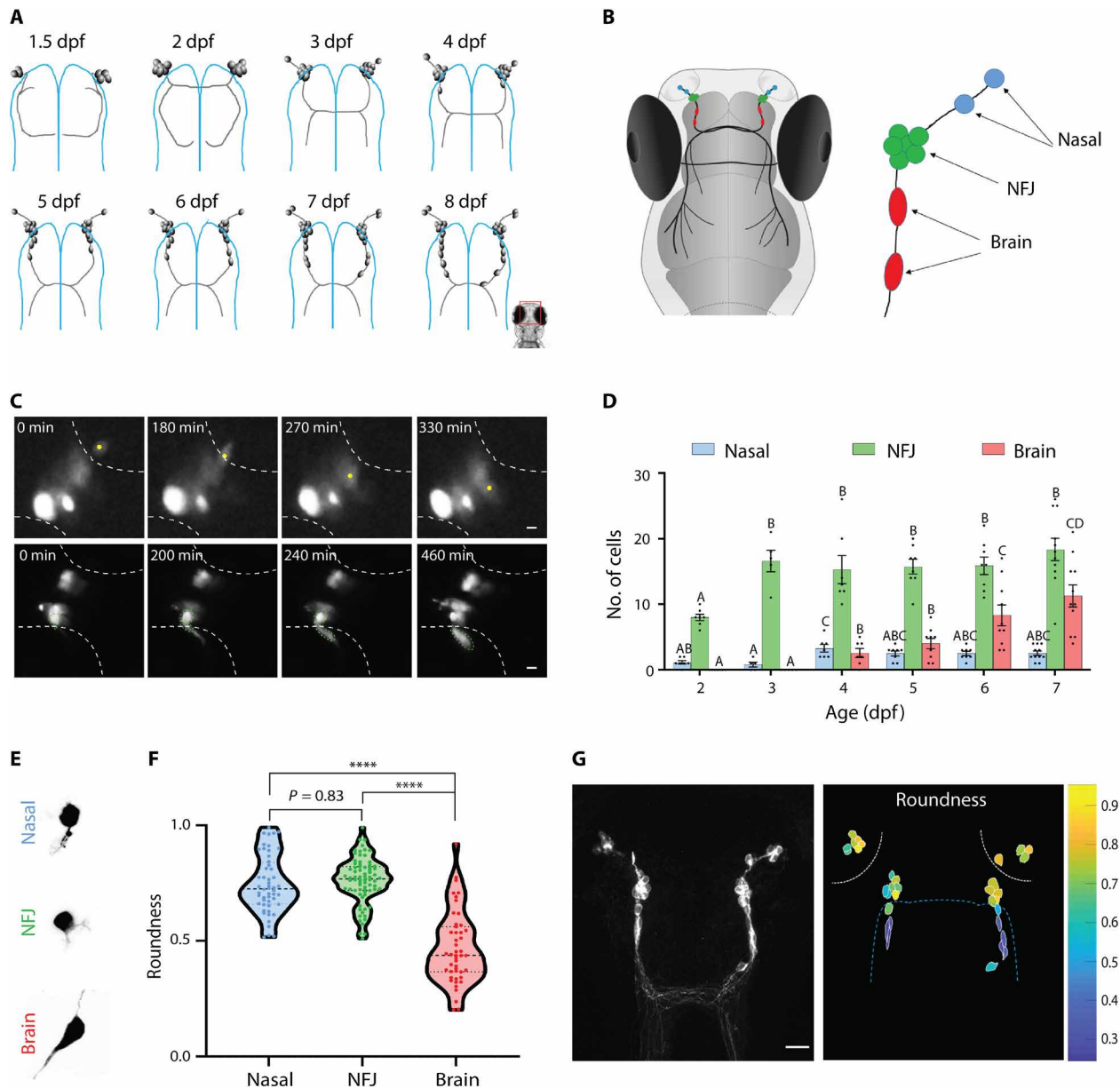


**Fig. 1. Migrating GnRH neurons pause for 3 days at the entrance to the brain and change their morphology.** (A) Schematic representation of the development of the zebrafish GnRH3 circuit during the first 8 days of development. Blue lines mark the boundary of the brain. (B) A schematic drawing of the migration path of GnRH3 neurons from the NP into the brain. An inset on the right describes the different location categories of the cells. (C) Snapshots from a 24-hour recording of a Tg(GnRH3:GFP) zebrafish larva showing the migration of a nasal GnRH cell (yellow dot, top) into the NFJ cluster and two NFJ GnRH cells (marked by green dashed lines, bottom) into the brain (see also movies S2 and S3, respectively). White dashed lines mark the border of the nasal (top) and brain (bottom) regions. Scale bars, 5  $\mu$ m. (D) Quantification of the migration process through the three different categories [ $n = 7, 5, 7, 8, 8,$  and 11 fish for 2 to 7 dpf, respectively]. Comparisons between cell numbers per fish were made within categories using one-way analysis of variance (ANOVA), followed by Dunnett's T3 multiple comparisons test. Different letters mark significantly different values ( $P < 0.05$ ). (E) Typical cell morphologies of nasal (top), NFJ (middle), and brain (bottom) cells. (F) Quantification of the roundness of cells in the different categories ( $n = 52$  nasal, 74 NFJ cells, and 47 brain cells; one-way ANOVA followed by Dunnett's T3 multiple comparisons test) \*\*\*\* $P < 0.0001$ . (G) An example of the morphological transition of GnRH3 cells. Left: A raw image of GnRH3 cells at 7 dpf [Tg(GnRH3:R-CaMP2)]. Scale bar, 20  $\mu$ m. Right: Individual cells traced and color-coded according to their roundness. White dashed lines mark the olfactory epithelium; blue dashed line marks the brain border.

projections within the GnRH3 circuit. Hence, our data suggest that new GnRH neurons migrating from the NP become coordinated with other GnRH neurons only when they contact NFJ GnRH neuronal clusters, while brain GnRH neurons remain coordinated with NFJ GnRH neurons.

### The developing GnRH3 circuit is functionally isolated

To understand whether the observed coordination is a result of internal connectivity, we used a combination of postsynaptic labeling, transsynaptic tracing, and functional calcium imaging. First, we followed the dendritic tree of GnRH neurons by sparsely transfecting

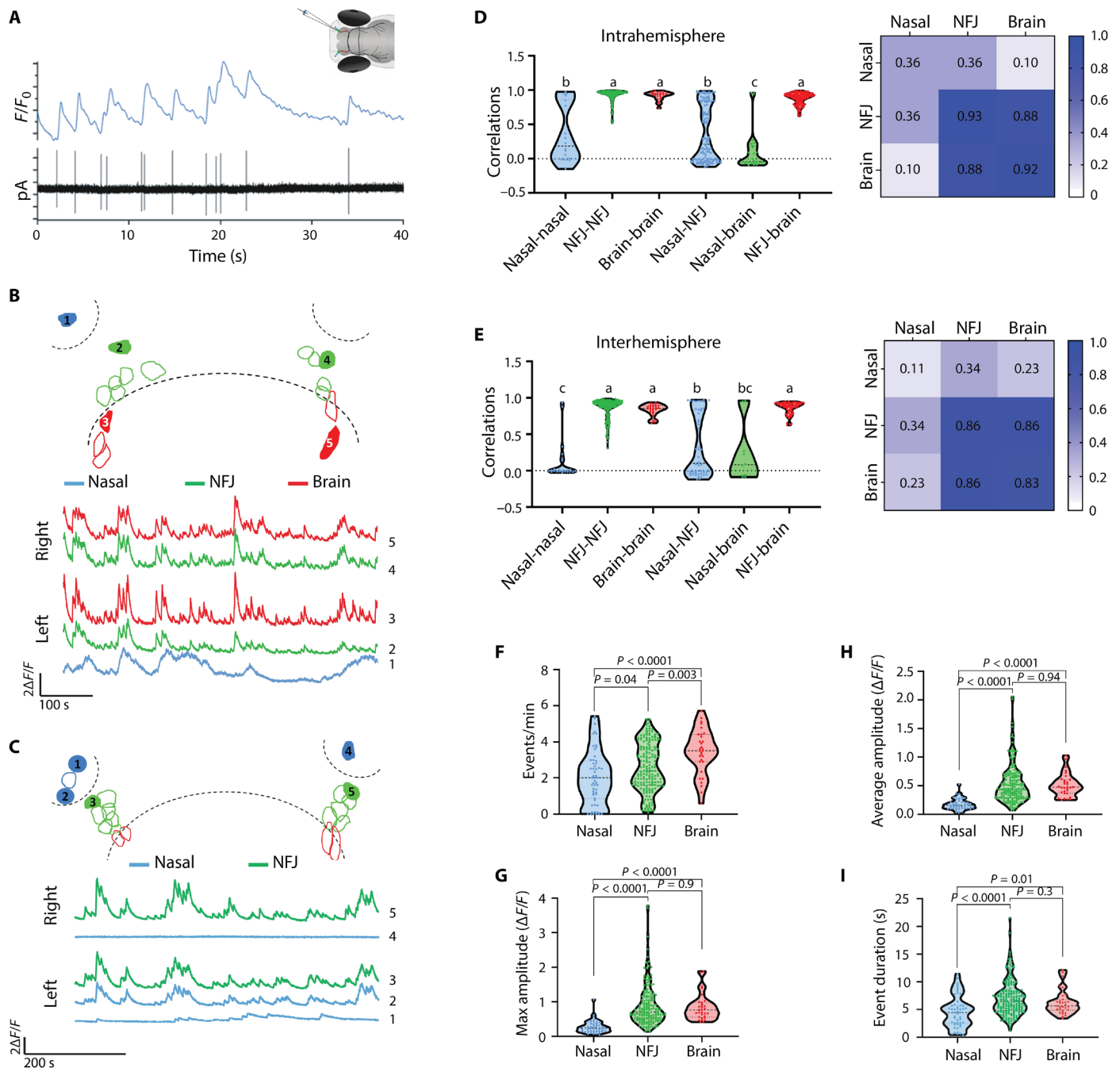


**Fig. 2. Migrating GnRH3 neurons become functionally coordinated upon reaching the NFJ cluster.** (A) Simultaneous calcium imaging [Tg(GnRH3:R-CaMP2)] and in vivo loose-patch recording of a GnRH3 neuron (3 dpf) reveal a strong correlation between electrical activity [picoamperes (pA), bottom trace] and calcium (top trace). (B and C) Example calcium traces of five cells from 6-dpf larvae (also see movies S4 and S5, respectively). Red traces are brain cells, green traces are NFJ cells, and blue traces are nasal cells. Top traces are cells on the right hemisphere; bottom traces are cells from the left hemisphere. A scheme above each trace depicts the imaged circuit, with dashed lines marking the nasal and brain borders. Numbered traces correspond to the cells marked in the scheme and in fig. S5 (A and B). Bars:  $2\Delta F/F$ , 100 (B) or 200 s (C). (D) Left: Pairwise Pearson's correlation of calcium traces from nasal, NFJ, and brain cells within the same hemisphere. Different letters indicate significantly different means ( $n = 55$  nasal cells, 181 NFJ cells, and 31 brain cells from 15 6-dpf fish; one-way ANOVA followed by Dunnett's T3 multiple comparisons test). Right: A correlation matrix of intrahemisphere correlations. Numbers indicate mean correlation value. (E) Interhemisphere correlations. Details as in (D). (F to I) Calcium activity parameters of nasal, NFJ, and brain GnRH neurons at 6 dpf. Statistics as in (D).

GnRH3 neurons with the postsynaptic density protein 95 (PSD-95) fused to green fluorescent protein (GFP) to label active postsynaptic sites (32). Although clustered NFJ GnRH3 neurons send long and branched projections into the brain (fig. S8), PSD-95 distribution was limited to a small area of the soma and to a short neurite that is usually contained within the NFJ cluster (Fig. 3A), implying an internal source of input. To identify possible synaptic partners, we expressed the transsynaptic tracer wheat germ agglutinin (WGA) (33) and GFP specifically in GnRH3 neurons [Tg(GnRH3:gal4ff; UAS:AcGFP-T2A-WGA)]. However, WGA staining was not found outside of the GnRH3 circuit in young (7 dpf) fish, suggesting the lack of functional communication between GnRH and non-GnRH cells at this developmental stage (fig. S9A). At the age of 14 dpf, a time when the first GnRH3 neurons send projections to the pituitary (21), we begin to observe WGA staining on non-GnRH cells within the olfactory lobes (fig. S9B) and in the subpallium, around the anterior commissure (fig. S9C). This pattern becomes more pronounced at later stages (fig. S9D). To further explore whether the circuit of migrating GnRH neurons is functionally connected with non-GnRH neurons, we performed two-photon calcium imaging of large neuronal populations (expressing GCaMP5G under the control of the pan-neuronal HuC promoter) while simultaneously monitoring the activity of the NFJ and brain GnRH3 neurons (labeled red by R-CaMP2) at 6 to 8 dpf. Mapping the correlation levels onto the anatomical maps of the brain revealed a high level of coordinated activity between NFJ and brain GnRH neurons compared to non-GnRH cells (Fig. 3B), which suggests that both NFJ clusters and brain GnRH neurons function during the first stages of development as an isolated, autonomous circuit of interconnected GnRH neurons.

### GnRH3 neurons communicate synaptically through glutamatergic activation of NMDA receptors

We explored the nature of the connectivity between GnRH3 neurons by sparsely transfecting GnRH3 neurons with a bicistronic construct driving the expression of the transsynaptic tracer WGA (33) and mCherry (GnRH3:WGA-T2A-mCherry). Transfection of single cells, marked by the expression of mCherry, caused all the cells within the ipsilateral hemisphere to stain positive for WGA at 7 dpf (Fig. 3C). Moreover, transfection of single cells in one hemisphere also caused WGA transfer to cells in the contralateral hemisphere (Fig. 3D), indicating that GnRH3 cells both within and between the two hemispheres are connected by chemical synapses. The synaptic nature of the connectivity between GnRH neurons was further supported by immunohistochemical staining of GnRH3 varicosities juxtaposed onto other GnRH3 cells by the presynaptic marker synaptophysin (Fig. 3E and fig. S10). To specifically block synaptic transmission between GnRH3 neurons, we generated a transgenic line expressing botulinum toxin (botox) light chain in GnRH3 neurons [Tg(GnRH3:gal4ff; UAS:Botox)]. In this line, botox expression could be detected in  $52.70 \pm 7\%$  of GnRH neurons (Fig. 3F). Calcium imaging of NFJ GnRH neurons in these fish showed a sharp decrease in coordination between the two hemispheres and a slight decrease in the intrahemisphere coordination levels (Fig. 3, G to I;  $n = 7$  wild-type fish and 9 botox fish). This suggests that the low percentage of botox-expressing cells was not enough to completely block intrahemisphere communication between NFJ GnRH neurons but was sufficient to uncouple the weaker connection between the two hemispheres. Together, these results suggest that the coordination between GnRH neurons is driven through internal chemical synapses.

Since GABAergic and glutamatergic signaling have been reported in migrating GnRH neurons (5, 34), we crossed Tg(GnRH3:GFP) fish to fish expressing DsRed under the *gad1b* or the *Vglut2A* promoters to identify the neurotransmitter by which GnRH3 neurons communicate. We found no colabeling of *gad1b* in NFJ GnRH3 neurons nor did the  $\gamma$ -aminobutyric acid type A receptor antagonist picrotoxin affect their coordinated calcium activity (fig. S11). In contrast, GnRH3 neurons were found to express *Vglut2A* in 39 to 53% of the cells (Fig. 4, A to C, and fig. S12) as well as the NMDA receptor subunits NR1 and NR2D (Fig. 4D and fig. S13). NMDA receptors usually require an initial depolarizing step, provided by AMPA receptors, to dislodge the magnesium ion from the channel. However, NMDA receptors that contain the NR2D subunit can operate at resting potential and therefore do not require this initial depolarization step (35, 36). To explore the functional role of the glutamatergic communication, we injected either the AMPA receptor antagonist 6-cyano-7-nitroquinoxaline-2,3-dione (CNQX) or the NMDA receptor antagonist 2-amino-5-phosphonopentanoic acid (AP-5) into the circulation of 3- or 6-dpf larvae and recorded calcium activity using GCaMP6s (Fig. 4E). CNQX slightly increased intra- and interhemisphere communication at 3 dpf (Fig. 4, F and G) and slightly decreased interhemisphere correlation levels at 6 dpf (Fig. 4, H and I). By contrast, injection of AP-5 had a profound effect on cell-cell communication between GnRH3 neurons (Fig. 4E), markedly decreasing both the intra- and interhemisphere coordination levels ( $P < 0.0001$ ; Fig. 4, F to I) at both ages (3 dpf:  $n = 6, 6$ , and 8 fish for saline, CNQX, and AP-5, respectively; 6 dpf:  $n = 7$  fish for all treatments). The AP-5 treatment also significantly dampened the frequency, amplitude, and duration of calcium transients and completely silenced 19 and 35% of the cells at 3 and 6 dpf, respectively (Fig. 4, J to M, and fig. S14). Notably, AP-5 treatment could suppress synchronized calcium transient firing in NFJ neurons, while it failed to alter asynchronous calcium signals in nasal cells (fig. S14). Together, these results suggest that both the initiation of neuronal firing and neuronal synchronization and the digital and amplitude coding of calcium transients within the circuit of NFJ GnRH neurons depend on glutamatergic activation of postsynaptic NMDA receptors.

### GnRH3 neurons are reciprocally wired between the two NFJ clusters

The drastic effect of NMDA blockers on both the coupling of NFJ GnRH neurons and their calcium activity (Fig. 4, E to M) suggested to us that the two aspects were intermingled. Spontaneous activity as an emergent property of a network was already reported in other developing neurons where coincident integration of excitatory synaptic inputs initiates spike firing in randomly distributed neurons which then propagates throughout the population [so-called integrate-and-fire cell model (37–39)]. Such systems require strong reciprocal connections between the cells (40). Optogenetic control of membrane excitability in distinct neurons allowed us to probe the connectivity patterns in clusters of NFJ GnRH neurons in which light activation of depolarizing opsins was used to mimic coincident excitatory inputs. We therefore optogenetically stimulated single channelrhodopsin2 (ChR2)-expressing NFJ GnRH3 neurons using two-photon microscopy while recording the calcium response of neighboring cells using R-CaMP2 at 3 and 7 dpf (Fig. 5, A and B). Four stimulation events were applied in 30-s intervals. At the ipsilateral (ipsi) hemisphere level, sequential ChR2-driven depolarization of distinct NFJ GnRH neurons (71% of stimulated neurons) leads to neuron

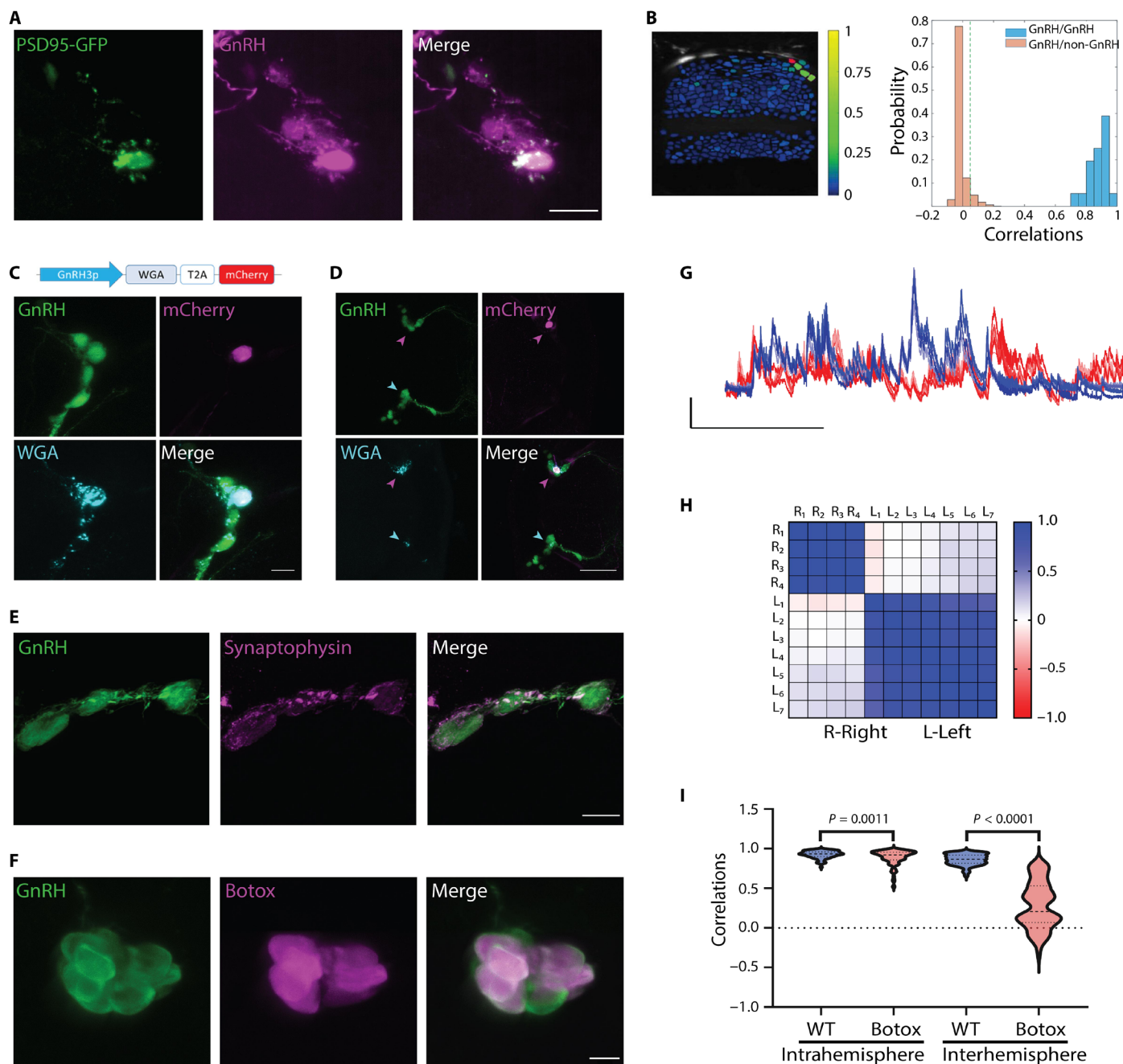


**Fig. 3. GnRH3 neurons are functionally isolated and synaptically wired.** (A) An example of the short dendritic tree of a single GnRH3 neuron marked by GFP-PSD95 (green), contained within the GnRH3 circuit (magenta). Scale bar, 10  $\mu$ m. (B) Left: Example activity correlation map of developing NFJ and brain GnRH neurons (7 dpf, circled in magenta) with other neurons of the telencephalon. Recording was performed on Tg(HuC:GCaMP5G) larvae that expressed GCaMP5G in all neurons. Right: Correlation distributions of GnRH neurons versus other GnRH neurons (blue) or versus non-GnRH neurons (brown). The null-model derived threshold (fig. S20) is depicted as a green dashed line ( $n = 5$  fish, 6 to 8 dpf). (C) Sparse labeling of a 7-dpf Tg(GnRH3:GFP) fish (green) with GnRH3:WGA-T2A-mCherry construct results in transfection of a single neuron (magenta). WGA (cyan) can be observed in all other cells within the hemisphere. Scale bar, 10  $\mu$ m. A scheme of the construct used for sparse labeling. (D) Transfection of a single cell on the right hemisphere (magenta arrowheads) resulted in WGA transfer to the contralateral side (cyan arrowheads). Scale bar, 50  $\mu$ m. (E) Immunostaining of synaptophysin (magenta) shows GnRH3 neurons (green) forming multiple synapses upon each other. Scale bar, 10  $\mu$ m. (F) Expression of botox (magenta) in GnRH neurons (green). Note that not all GnRH cells express botox. Scale bar, 10  $\mu$ m. (G) Calcium traces recorded from GnRH neurons of a 3-dpf botox-positive larva show uncoupling of activity between the left (red traces) and right (blue traces) hemispheres. Bars:  $\Delta F/F$ , 200 s. (H) Correlation matrix of the cells from the same fish in (G). (I) Quantification of correlation of NFJ cells from botox and control fish shows a slight reduction in correlation within clusters and a sharp decrease in correlation between the two hemispheres ( $n = 7$  wild-type fish and 9 botox fish, unpaired  $t$  test with Welch's correction). WT, wild type.

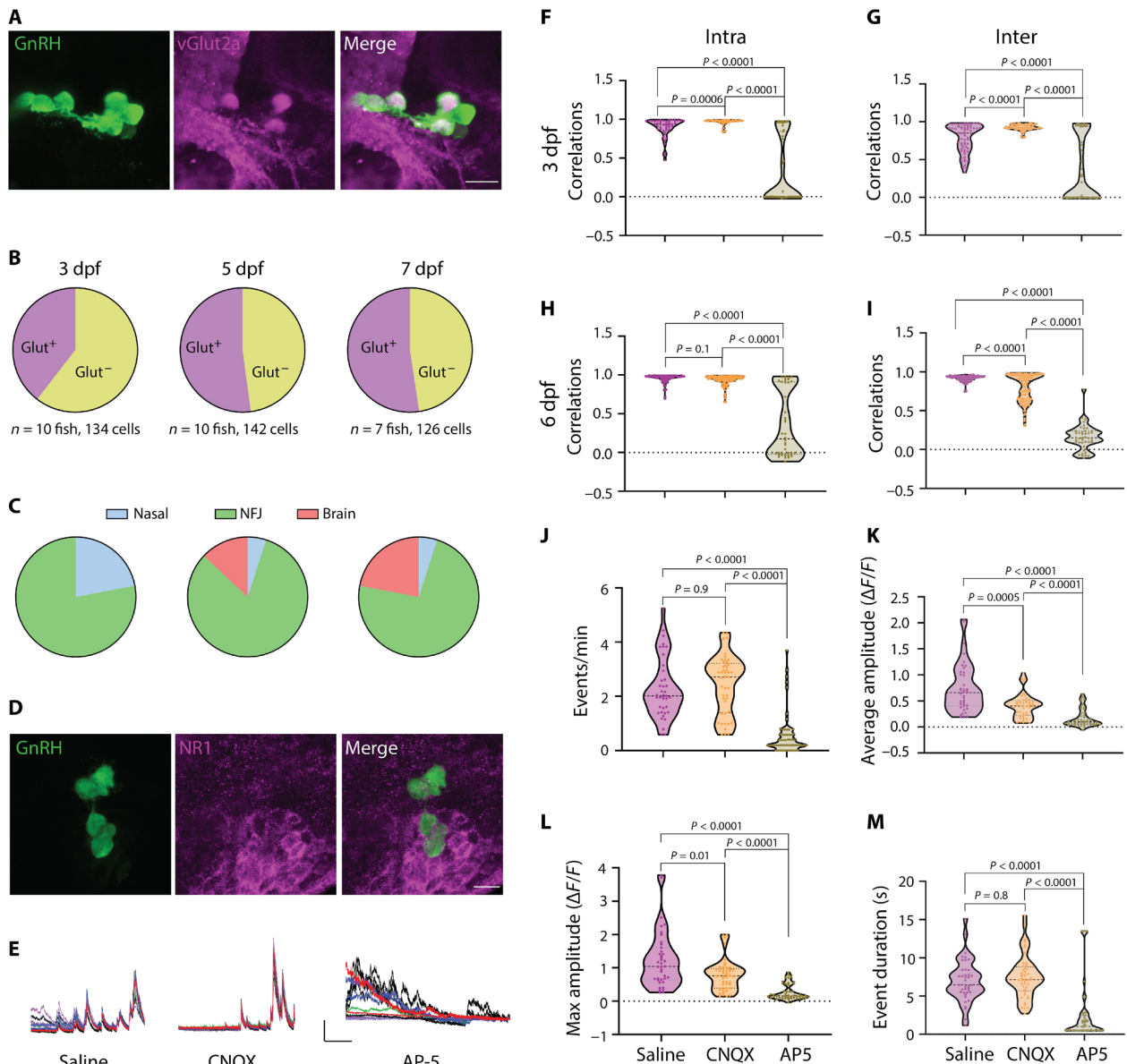


**Fig. 4. Developing GnRH3 neurons communicate through glutamatergic transmission.** (A) Crossing Tg(GnRH3:GFP) and Tg(vGlut2a:DsRed) fish reveals coexpression of vGlut2a in NFJ GnRH3 cells (7 dpf). Scale bar, 10  $\mu$ m. (B) Quantification of the percentage of DsRed-positive GnRH3 neurons for each age (*n* numbers are given on the figure). (C) The distribution of DsRed-positive GnRH3 cells within the different migration categories for each age. (D) Colocalization of NMDA receptor NR1 on GnRH neurons (3 dpf). Scale bar, 10  $\mu$ m. (E) Example calcium traces obtained from 6-dpf larva injected with saline, CNQX, or AP-5. Bars:  $2\Delta F/F_0$ , 50 s. (F to I) Comparison of intra- (F and H) and interhemisphere (G and I) pairwise Pearson's correlations of the different treatments at 3 (F and G) and 6 (H and I) dpf (3 dpf: *n* = 39, 45, and 58 cells from = 6, 6, and 8 fish for saline, CNQX, and AP-5, respectively; 6 dpf: *n* = 52, 64, and 50 cells from 7 fish for each treatment; one-way ANOVA followed by Dunnett's T3 multiple comparisons test). (J to M) Comparison of calcium activity parameters from 3-dpf larvae (*n* = 39, 45, and 58 cells from = 6, 6, and 8 fish for saline, CNQX, and AP-5, respectively).

activation and coordinated calcium transients with GnRH neighbors (Fig. 5A, *n* = 35). Moreover, we observed no directionality in the activation patterns of the cells, suggesting that calcium transients can be elicited from multiple neuronal entities within NFJ clusters. The two contralateral hemispheres were also reciprocally responsive to stimulation, although responses in the contralateral hemisphere were recorded only in 26% of the cases (Fig. 5B, *n* = 19), reflecting a lower strength of synaptic connectivity between the hemispheres than within a hemisphere (Fig. 3, F to I), probably resulting from the scarcity of intercluster projections (only 7%; fig.

S8). Electrical stimulation of GnRH3 neurons reproduced the responses observed with photostimulation (fig. S15, *n* = 4 fish). Hence, these data strengthen the proposal that depolarizing events due to coincident glutamatergic inputs could lead to spike initiation that propagates throughout the GnRH circuit to generate synchronized calcium transients (schematized in Fig. 5, C and D).

To further address the importance of the interhemisphere connectivity, we laser ablated the NFJ cluster of one hemisphere while monitoring calcium signals in GnRH neurons of the contralateral hemisphere. Acute ablations caused a cessation of calcium activity





developing GnRH neuron circuit and highlights the plasticity and robustness of the circuit.

### Circuit-intrinsic control of GnRH neuron migration

Last, we explored the functional role of neuronal activity and interconnectivity on the migration of zebrafish GnRH3 neurons. Since GnRH neural activity is an emergent property of the network, we sought to simulate the activity-dampening effects of reduced connectivity in individual GnRH neurons and test the effect on their migration. To silence the cells, we sparsely expressed the inward-rectifying potassium channel Kir2.1 in GnRH3 neurons (Fig. 6A). Kir2.1 hyperpolarizes the cells, hence effectively silencing them (43). Calcium imaging confirmed effective silencing of Kir2.1-expressing cells while not affecting the activity of the nontransfected GnRH3 cells (Fig. 6B). Quantifying the migration after 7 days (Fig. 6C), we found that Kir2.1-expressing cells traveled a significantly shorter distance than their nontransfected counterparts, resulting in a skewed distribution along the migration path and a significantly lower number of cells entering the brain (35 transfected and 335 nontransfected cells from 22 fish; Kolmogorov-Smirnov test,  $P < 0.0001$ ; Fig. 6, D and E). These results indicate that the ability of GnRH neurons to enter the brain depends on their electrical integration into the NFJ clusters. Conversely, overexpression of a mutant, nonactive Kir2.1, did not affect migration (27 transfected and 180 nontransfected cells from 13 fish; Kolmogorov-Smirnov test,  $P = 0.97$ ; fig. S17). To perturb GnRH3 connectivity, we blocked NMDA-mediated glutamatergic transmission using the NMDA antagonist MK-801. Since MK-801 can cross the blood-brain barrier, it can be applied in the rearing medium of the fish. MK-801 (50  $\mu\text{M}$  for 3 hours) decreased the coordination of calcium transients of GnRH3 neurons (fig. S18). When applied between 3 and 6 dpf, MK-801 caused a significant decrease in the number of GnRH cells entering the brain (fig. S18;  $n = 19, 16, 11,$  and  $11$  fish per treatment for 0, 20, 50, and 200  $\mu\text{M}$ , respectively). While the developing GnRH circuit is functionally isolated at these stages, we cannot rule out the possibility that part of the effects may be attributed to global effects of the prolonged drug treatments. Together, these results suggest that the connectivity-dependent activity of GnRH3 neurons is necessary for the cells to acquire the ability to leave the NFJ and enter the brain.

### DISCUSSION

By combining live-imaging of migrating GnRH3 neurons in awake fish larvae together with monitoring and manipulating the dynamics of their calcium signals, we developed an approach to decipher why GnRH3 neurons pause at the entrance to the brain. A shift in the morphology of GnRH3 neurons upon entering the brain marks the pause as an important transition period for the cells. Our data suggest that connectivity and synchronized firing of NFJ GnRH neurons during the migrational pause drive the morphological transition of GnRH neurons that will leave the NFJ cluster. As GnRH3 cells pause at the entrance to the brain, they form interconnections between clusters located at the base of both hemispheres. These two NFJ GnRH clusters communicate via homotypic NMDA-driven synaptic contacts leading to both the emergence and propagation of within-population co-active, high-amplitude calcium transients that are scaled at the interhemisphere level with functional connection with migrating brain GnRH neurons on both ipsi- and contralateral sides. Ultimately, the coordinated spontaneous activity acts

as a gatekeeper by mediating a critical transition in GnRH neurons, which enables them to enter the brain and migrate toward their hypothalamic destination (summarized in Fig. 6F).

The pause in migration and clustering of GnRH neurons at the cribriform plate were described in several tetrapods (4, 5, 44), yet without the *in vivo* context, the function of these neuron clusters remained unknown (45). Our live imaging approach reveals that the sojourn of GnRH neurons at the “waiting compartment” is accompanied by an emergence of synchronized, high-amplitude calcium transients. Blocking these transients by silencing the cells prevents them from going through the necessary transition that is required for entering the brain. In this context, it has been previously shown that calcium influx through NMDA receptors forms an important bridge between the subsecond time scale of neural activity and the hours-long migration process by activating posttranslational modifications of proteins and affecting mRNA transcription (16, 46). Neuronal excitability and the ensuing fast calcium spikes have been reported to cause transcriptional modifications leading to morphological changes and migration arrest (17, 18). In GnRH neurons, NMDA receptor signaling to the nucleus through the NSMF gene (47) is a possible candidate for linking neural activity and migration since mutations in this gene are implicated in GnRH migration defects and infertility in humans (48, 49). Moreover, coordinated activity of GnRH cells has been observed in mammalian GnRH cell lines as well as in organotypic cell cultures (50, 51), suggesting that coordinated calcium activity exists in migrating GnRH neurons of higher vertebrates and may be relevant for their migration (14). Although the full molecular details of the maturation process that GnRH cells undergo during their phenotypic switch remain unknown, we hypothesize that their connectivity and cooperativity may match with the combinatorial expression of guidance molecules that direct GnRH migration and ultimately underlie the decision of individual cells to break away from the NFJ clusters.

Our discovery that the synchronized activity is mediated through chemical synaptic transmission is surprising since synaptogenesis is believed to take place only after migration is over, and the effects of neurotransmitters on migration (10, 11) are thought to be mediated through extrasynaptic receptors in a paracrine fashion (52). Yet recently, subplate neurons were shown to use transient chemical glutamatergic synapses to facilitate the multipolar-to-bipolar transition of migrating neocortical neurons (8). As in the case of the zebrafish GnRH3 neurons, subplate neurons use postsynaptic NMDA receptors to mediate the communication and drive the morphological transition (8). However, unlike subplate neurons, zebrafish GnRH3 neurons exert control over their own migration in a cell-autonomous manner. This cooperative and internal control of neuronal migration supplements the traditional view according to which migration is mostly a consequence of the interplay between individual GnRH cells and external cues, which include adhesion molecules, growth factors, and neurotransmitters. By driving the phenotypic switch of GnRH neurons, the activity-dependent regulation of migration grants the developing circuit control over its own assembly. Therefore, its internal wiring patterns, synchronized activity, and functional isolation during the initial stages of the circuit assembly make the migrating GnRH3 system a bona fide self-organizing circuit.

We demonstrate that co-activity within the GnRH circuit depends on excitatory inputs, which emanate from multiple neuronal entities within the NFJ GnRH clusters. The almost complete cessation of activity upon blocking postsynaptic transmission suggests

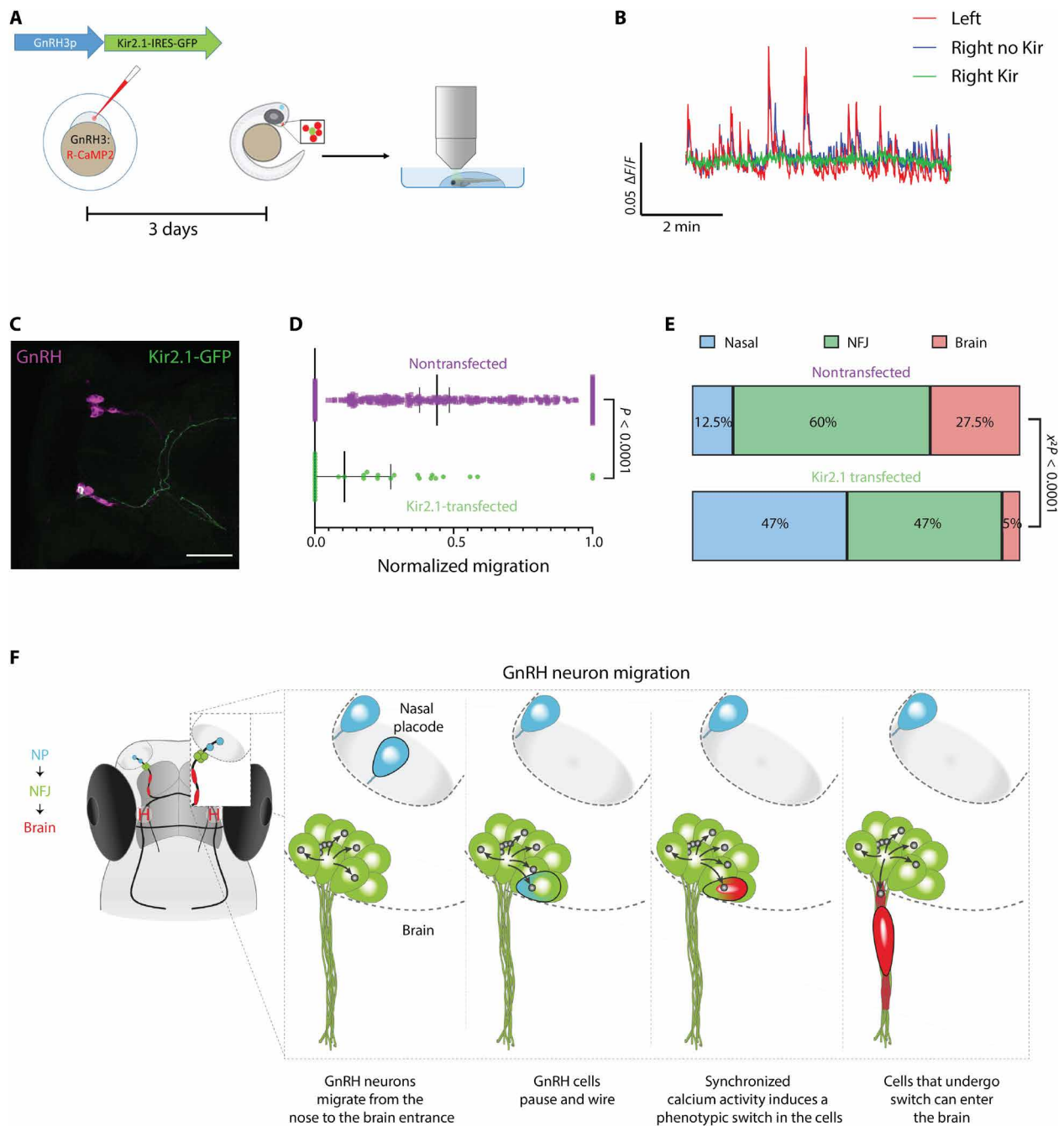


**Fig. 6. Control of GnRH neuron migration by their excitability.** (A) Scheme of silencing strategy: Individual GnRH3 neurons were silenced by sparse expression of Kir2.1, followed by calcium imaging and quantification of migration. (B) Calcium imaging of a Kir2.1-overexpressing neuron (green) within the GnRH3 circuit (blue and red traces are nontransfected cells) at 3 dpf shows effective silencing of the Kir2.1-expressing cell. (C) A Kir2.1-transfected neuron (green) within the GnRH circuit (magenta) at 7 dpf. Scale bar, 50 μm. (D) At 7 dpf, overexpression of Kir2.1 significantly reduces the distance migrated by GnRH3 cells ( $n = 35$  transfected and 335 nontransfected cells from 22 fish; Mann-Whitney test,  $P < 0.0001$ ; distance was normalized to maximal distance migrated by a GnRH cell in the same fish) and skews their distribution along the migration pathway (Kolmogorov-Smirnov test,  $P < 0.0001$ ). (E) Relative frequency of Kir2.1-overexpressing cells and nontransfected cells within the three cell categories at 7 dpf. Kir2.1-overexpressing cells are less likely to become brain cells. Similarly, less Kir2.1-overexpressing nasal cells integrate the NFJ clusters [ $n$  numbers as in (D)].  $\chi^2$  test of distributions]. (F) A graphical model illustrating the migration of a single GnRH3 neuron (marked by black border) from the NP into the zebrafish brain. Nasal, NFJ, and brain GnRH neurons are pseudo-colored in blue, green, and red, respectively. The blue-green and green-red color codes illustrate the transition of the single GnRH3 neuron (marked by black border) as it becomes synaptically connected with other NFJ neurons (arrows, neurite connection; dot, glutamatergic synapse) and changes its morphology before leaving the NFJ cluster, respectively.

that synaptic connection is at the core of localized spike initiation. The synaptic-dependent emergence of spontaneous and coordinated activity is a hallmark of developing neural networks. In these networks, there is no real need for pacemaker/leader neurons to drive the rest of the population as followers (37–39). We therefore propose that synaptic glutamatergic connections generate sub-threshold noise, which is accumulated and integrated to trigger a randomly localized cell, which then propagates toward neighboring GnRH neurons (37). In such “integrate-and-fire” networks, activity and coordination are difficult to dissociate, as synaptic connectivity is both necessary and sufficient to allow the emergence of spontaneous synchronized activity (38, 39).

An added feature of such a reciprocal network structure with multiple activity drivers is increased robustness and redundancy since elimination of a single GnRH neuron, or even several neuronal entities, will not significantly affect the function of the system. This illustrates the robustness of the GnRH circuit, which is strongly internally wired and does not get interference from other neuron neighbors in the developing brain. Such a high level of robustness is likely necessary for a system that is responsible for the propagation of the species. Mammalian studies have shown that animals remain fertile even after a loss of up to 88 to 66% of GnRH neurons (53), suggesting an exceptionally high level of redundancy and robustness within the GnRH circuit. Our study reveals a similar trend during GnRH neuron development.

Together, our data unveil an interhemisphere, circuit-intrinsic control of GnRH neuron migration where synaptically driven synchronized activity mediates a phenotypic switch, which is mandatory for proper migration toward their final hypothalamic destination. We propose an updated model for GnRH neuronal migration, critical for vertebrate reproduction and species survival, in which GnRH neurons function as a population rather than as individual units. By implementing recently reported methods of regionally specified human pluripotent stem cell–derived organoids (54), our findings provide a previously unidentified template for exploring the underlying forces controlling the assembly of the human GnRH circuit in health and disease.

## MATERIALS AND METHODS

### Experimental design

The aim of the current study was to investigate the role of cell-cell communication in the regulation of GnRH neuronal migration. To that end, we adopted a transgenic zebrafish model that uses the zebrafish GnRH3 promoter to drive expression of foreign proteins specifically in GnRH3 cells. Our work was based mostly on non-invasive *in vivo* imaging of intact fish larvae using two-photon microscopy. Zebrafish were chosen because of their external development, transparency, small size, and rich transgenic toolbox that make them particularly attractive for *in vivo* imaging of developmental processes. Part of the experiments were conducted on stable transgenic lines, whereas others used sparse labeling of individual GnRH3 neurons or the combination of the two. All experiments were performed on larvae between 1 and 7 dpf, before the onset of external feeding. To increase larval transparency and to avoid the need to inhibit pigment formation by pharmacological means, all experiments were performed on nacre (*mitfa*<sup>-/-</sup>) background that lack melanocytes. Since work was conducted on larvae, sex cannot be determined for the subjects. Age of larvae is specified for each experiment

in the manuscript. Experimental units throughout the study were either individual larvae or GnRH cells, dependent on the particular experiment.

### Sample size and replication

Since this was our first attempt at recording spontaneous calcium activity in zebrafish GnRH3 neurons, we relied on preliminary experiments to characterize the system and determine the correct sample size. For calcium imaging experiments, five fish were chosen as the minimum number of replicates used for analysis, and sample size was determined according to the number of GnRH cells in these fish. GnRH cells within a fish showed high uniformity in their activity patterns.

### Data inclusion/exclusion criteria

Larvae were excluded from analysis if the fish showed no spontaneous calcium activity (usually less than 5% of larvae tested) or if fish movements during the full recording session prevented reliable calcium readout. Data or samples were not excluded from analysis for other reasons.

All replication attempts were successful. Calcium patterns, number and shape of cells, and treatment effects were consistent across the study period. For optogenetic stimulation, the percentages of successful versus unsuccessful stimulation attempts are depicted in Fig. 5.

### Randomization

Fish used for the experiments were randomly selected and randomly assigned to experimental groups. All GnRH cells that could be detected in the selected fish were used for analysis, and thus, there was no requirement for randomization of cell selection.

### Blinding

During experimentation and data acquisition, blinding was not purposely introduced into the work scheme as a mean to ensure correct tractability of the samples. Quantifications of calcium data were performed using a computational pipeline applied equally to all samples.

### Animals

All experiments were approved by the Animal Welfare and Ethical Review Body of Languedoc-Roussillon (APAFIS#745-2015060114396791 v3). Zebrafish were housed according to standard conditions. Fertilized eggs were incubated at 28.5°C in E3 medium. Transgenic lines generated for the current study are Tg(GnRH3:GFP), Tg(GnRH3:R-CaMP2), Tg(GnRH3:gal4ff), Tg(UAS:Botox), and Tg(GnRH3:Chr2-YFP). Transgenic line generation was described elsewhere (55). Other lines used were Tg(VGlut2A:DsRed), Tg(Gad1B:DsRed), Tg(UAS:Kaede), and Tg(HuC:GCaMP5G) (56). Line Tg(UAS:AcGFP-T2A-WGA) (57) was a gift from Y. Yoshihara (RIKEN Brain Science Institute, Japan). Line Tg(UAS:GCaMP6s) (58) was a gift from H. Baier (Max Planck institute of Neurobiology, Germany). Line Tg(UAS:NTR-mCherry) was a gift from G. Lutfalla (University of Montpellier, France).

### Plasmid construction

All expression plasmids were generated using the Tol2kit (21) and Gateway system (Invitrogen). Briefly, entry clones were generated by addition of appropriate adaptors to DNA fragments via polymerase chain reaction (PCR) amplification. Amplicons were then recombined into donor vectors using BP recombination. A 5'-entry clone (p5E), a middle entry clone (pME), and a 3'-entry clone (p3E) were then recombined through an LR reaction into an expression

vector carrying tol2-recognition sequences and either an mCherry or a GFP heart marker. The GnRH3 promoter (20) was cloned from zebrafish genomic DNA and inserted into pDONRP4-P1R to generate p5'-GnRH3. R-CaMP2 (59) was a gift from H. Bitó (University of Tokyo) and was cloned into pDONR221 to generate pME-R-CaMP2. The BoTxBLC open reading frame (ORF) was cloned from genomic DNA of BoTxBLC-GFP (60), a gift from C. Wyart (Institut du Cerveau, Paris, France), and inserted into pDONR221 to generate pME-botox. Codon-optimized Gal4ff was cloned from Gal4ff.zf1, plasmid number 61392, a gift from H. Burgess (61), and inserted into pDONR221 to generate pME-gal4ff. The Kir2.1 ORF was cloned from mouse heart cDNA and inserted into pDONR221 to generate pME-Kir2.1. To mutate the Kir2.1 sequence, we used PCR-based site-directed mutagenesis on the pME-Kir2.1 to generate pME-mutKir2.1 (GYG144-146AAA). The WGA ORF without the stop codon was cloned from genomic DNA extracted from Tg(UAS:AcGFP-T2A-WGA) and inserted into pDONR221 to generate pME-WGA. 14xUAS PSD95:GFP 5UAS:DSRedExpress, plasmid number 74315, was a gift from M. Meyer and S. Smith (32).

### Immunohistochemistry

For whole-mount immunohistochemistry, larvae were fixed in 4% paraformaldehyde (PFA) in phosphate-buffered saline (PBS) overnight at 4°C. Larvae were then washed three times in PBS with 0.25% Triton X-100 (PBT) and permeabilized in 0.05% trypsin-EDTA on ice. After washing, samples were blocked with 2% donkey serum for 1 hour at room temperature and incubated overnight at 4°C with primary antibodies diluted in PBT + 1% bovine serum albumin and 1% dimethyl sulfoxide. Larvae were then washed in PBT and incubated with secondary antibodies at room temperature for 2 to 4 hours. Primary antibodies used were rabbit anti-red fluorescent protein (1:500; 632496, Clontech), chicken anti-GFP (1:500; ab13970, Abcam), goat anti-WGA (1:500; AS-2024, Vector Labs), sheep anti-*Clostridium botulinum* BoNT-B Light Chain antibody (1:500; AF5420, R&D Systems), rabbit anti-NR1 (1:200; 114011, Synaptic Systems), and anti-synaptophysin [1:200; S5768, Sigma-Aldrich (62)]. After staining, the lower jaw was carefully removed under a dissecting microscope, and fish were mounted and imaged from the ventral side using a confocal microscope (Leica SP8-UV).

### Calcium imaging

Nonanesthetized larvae (1 to 7 dpf) were embedded in a drop of 2% (w/v) low-melting agarose. Imaging experiments were performed on Tg(GnRH3:gal4ff; UAS:GCaMP6s) or Tg(GnRH3:R-CaMP2) larvae for single-color imaging or on Tg(HuC:GCaMP5G; GnRH3:R-CaMP2) for two-color imaging, all in nacre background (*mitfa*<sup>-/-</sup>) to avoid pigment interference during imaging. Fish over 4 dpf were immobilized using  $\alpha$ -tubocurarine (5 mM; Sigma-Aldrich), and recordings lasted for 5 to 20 min, in the absence of external sensory stimulation.

Single-color calcium imaging was performed using a FVMPE RS two-photon microscope (Olympus) setup with an InSight X3 femtosecond-pulsed infrared laser (Spectra-Physics) and a 25 $\times$ , numerical aperture 1.05 water-immersion objective (XLPLN25XWMP2, Olympus). The laser wavelength was tuned to 940 nm for GCaMP6s or to 1040 nm for R-CaMP2. Calcium signals were recorded by time-lapse acquisition using galvanometric scanning mode and conventional raster scanning with a frequency up to 6 to 8 Hz. Two-color two-photon calcium imaging was performed as in Boulanger-Weill *et al.* (56).

### Analysis of Ca<sup>2+</sup> imaging data

Processing of the genetically encoded calcium indicator fluorescence was performed using the toolbox previously described (63). Important parameters are summarized below. To detect movement artifacts, all frames with large deviations in the cross-correlation between successive frames ( $z$ -score smaller than  $-2$ ) were manually inspected. Frames with identified moving artifacts were discarded for subsequent analysis. For single-color imaging, regions of interest (ROIs) corresponding to each neuron in the imaged plane were manually drawn. For two-color imaging in Tg(HuC:GCaMP5G; GnRH3:R-CaMP2), ROIs corresponding to neurons were semi-automatically detected on a morphological basis using a watershed algorithm on time-averaged registered videos. ROIs were then manually curated, and GnRH3 cells were identified by their red-channel fluorescence. Significant transients were extracted from the green fluorescence fluctuations in an adaptive and unsupervised manner considering fluorescence noise and decay dynamics of the calcium reporter (64). We used a confidence threshold of 99% and a decay time of 1.1 s for GCaMP5G and 3.0 s for GCaMP6s (64). Nonsignificant portions of the  $\Delta F/F_0$  traces were then set equal to 0 in all subsequent analysis.

### Analysis of the pairwise correlations between neurons

Pairwise correlations were computed from the temporal Pearson's linear correlation  $P$  for all neuronal pairs as in Boulanger-Weill *et al.* (56). Only neurons with at least one significant calcium transient were considered. Briefly, for a pair of neurons  $i$  and  $j$ ,  $p(i,j)$  was computed using significant  $\Delta F/F_0$  values (see the previous section). Significant correlations were extracted by thresholding correlation values. The threshold was calculated on the basis of a surrogate dataset where the spontaneous Ca<sup>2+</sup> events time stamps were randomly permuted. We then calculated the 99th percentile value of the distribution of the correlations, which was defined as the threshold for each recording (fig. S20).

### Analysis of the activity parameters

Activity frequency was computed as the number of active frames per minute. For the other activity parameters, we detected Ca<sup>2+</sup> events (trains of successive active frames) and computed the average length of events, average maximum amplitude of events, and onset and offset time duration (from the first active frame to the maximum and from the maximum to the last active frame, respectively).

### Photostimulation

Larvae [Tg(GnRH3:ChR2-YFP; GnRH3:R-CaMP2), 3 to 7 dpf] were mounted as described for calcium imaging. Photostimulation experiments were performed on an FVMPE RS two-photon microscope (Olympus) combining two collimated lasers: an InSight X3 femtosecond-pulsed infrared laser (Spectra-Physics) and a Chameleon Ultra II femtosecond-pulsed infrared laser (Coherent) for imaging and photostimulation, respectively. ChR2-expressing neurons were photoactivated applying four iterations of 200 ms, 13 mW, at 920 nm, using tornado-scanning mode restricted to an ROI manually selected to target a single GnRH3 cell (for detecting intracellular connectivity) or a cluster (to study interhemisphere connectivity). For single-cell optogenetic stimulation, tornado (spiral-like) two-photon excitation of an optical slice with an estimate three-dimensional (3D) resolution (objective point spread function: 0.45 and 2.2  $\mu$ m in  $x/y$  and  $z$  axes, respectively) was routinely sufficient to trigger a calcium transient in the targeted ChR2-expressing GnRH neuron. The fact that in some neurons

(29%) optogenetic stimulation leads to a calcium transient with no transmission to neuronal neighbors further supports the reliability of our single-cell stimulation protocol. Each photostimulation event was followed by 30 s of calcium imaging using R-CaMP2 at 1040 nm at a frequency of 5 to 7 Hz.

### Laser photoablation

Tg(GnRH3:gal4ff;UAS:GCaMP6s) larvae (3 dpf) were mounted in 2% low-melt agarose and imaged under a two-photon microscope as described above. Five minutes of calcium imaging was performed (940 nm, 4 to 10 Hz) before ablation to record normal spontaneous activity. An ROI for photoablation was then manually drawn around a single GnRH3 NFJ cluster (one hemisphere). Thereafter, photoablation of GnRH3 cells was performed using 3-s pulses of high intensity laser irradiation (Chameleon Ultra II laser set to 910 nm and a power to 75% of laser transmittance, corresponding to 267 mW at the imaging plane) using the built-in “tornado” stimulation tool. The procedure was repeated until complete ablation was achieved. Calcium imaging (5 min) was conducted immediately after photoablation and once again after 24 hours (at 4 dpf).

### Larva injection

Larvae (3 or 6 dpf) were mounted in 2% ultralow melt agarose and kept under tricaine anesthesia (0.016%, w/v). Under a dissecting stereomicroscope, 8 to 12 nl of drug was injected through a microcapillary using a picospritzer into either the heart or the brain ventricle. Fish were then released from the agarose and allowed to recover in E3 medium until imaging. Substances injected were saline, CNQX (at 1 mM in saline), and AP-5 (at 5 mM in saline).

### Kaede photoconversion

Larvae [Tg(GnRH3:gal4ff; UAS:Kaede), 3 dpf] were mounted in 2% ultralow melt agarose onto glass-bottom petri dishes and kept under tricaine anesthesia (0.016%, w/v). A confocal microscope (Leica SP8) equipped with a 405-nm laser was used to perform the photoconversion. The 405-nm laser was set to 20% power simultaneously with excitation at 488 and 561, and light was collected at both the green and red channels. Photoconversion was monitored by the disappearance of the green signal and increase of the signal in the red channel. Fish were then released and allowed to recover in E3 medium and imaged again using a FVMPE RS two photon microscope (Olympus) after 24 and 48 hours.

### Electrophysiology

Whole zebrafish larvae (3 dpf) were immobilized by immersion in  $\alpha$ -bungarotoxin dissolved in E3 medium for 10 min. Paralyzed larvae were mounted in 1% agarose on a glass coverslip. Sample was fixed on the stage of an upright microscope (Axioskop FS2, Carl Zeiss) in artificial cerebrospinal fluid (ACSF). Borosilicate glass pipettes (6 to 8 megohm) were backfilled with ACSF and connected to the head stage of an EPC-10 amplifier (HEKA) to acquire and store data using Patchmaster 2x42 software. Patch pipette under positive pressure was introduced into the nostril of the larvae and gently positioned on a R-CaMP2-positive neuron within a NFJ cluster. GnRH neurons expressing R-CaMP2 were visualized using an EM-CCD camera (C9100, Hamamatsu). Neuronal activity was recorded in voltage-clamp mode, in a loose-patch configuration (30- to 150-megohm seal resistance) (65). For direct electrical stimulation, voltage steps (1 V during 1 s every 15 s) were applied by EPC-10 amplifier through the patch pipette (configuration loose patch).

Calcium activity was recorded at 5 to 10 Hz using HC Image Live software (Hamamatsu Photonics, Japan). Synchronization of both patch clamp and imaging recordings was performed through internal triggering.

### Sparse labeling and single-neuron tracing

Sparse labeling was achieved by injection of the expression plasmid (7 ng/ $\mu$ l) and transposase mRNA (25 ng/ $\mu$ l) into 4- to 8-cell embryos. This resulted in low number of transfected cells. Larvae were subsequently screened under a fluorescent microscope at 3 dpf, and only those with very sparse expression (one to two cells) were chosen for imaging. Tracing and reconstruction of individual GnRH3:GFP-labeled neurons were performed on 3D confocal stacks using the Simple Neurite Tracer tool on ImageJ.

### In situ hybridization

A fragment of the GnRH3 and NR2D genes was amplified from zebrafish brain cDNA with the addition of T3 and T7 promoters on the antisense and sense orientations, respectively. These fragments were used to transcribe Digoxigenin (DIG)-labeled probes using the RNA DIG labeling kit (Roche Diagnostics). Whole-mount in situ hybridization was performed on 3- to 5-dpf Tg(GnRH3:GFP) larvae as described by Thisse and Thisse (66) with slight modifications. These modifications were treatment of the embryos with hydrogen peroxidase [2% (v/v) in methanol] for 30 min and the addition of 5% (v/v) dextran sulfate to the hybridization mix. Fluorescent signal was developed using the TSA amplification kit (PerkinElmer) for GnRH and Fast Red for NR2D. Larvae were then washed in PBS and immunostained using chicken anti-GFP antibodies and secondary donkey anti-chicken Alexa Fluor 488 antibodies to visualize transgene expression. Double-labeled larvae were imaged on a confocal microscope (Leica SP8).

### CUBIC

Dissected brains from adult Tg(GnRH3:GFP) fish were fixed overnight in 4% PFA in PBS. Fixed brains were washed and transferred to CUBIC-1 buffer (67) for 6 hours. Brains were then mounted in CUBIC-1 buffer and imaged using a confocal microscope (Leica SP8).

### DiI retrograde labeling

Dissected heads from Tg(GnRH3:GFP) fish were fixed overnight in 4% PFA in PBS. Following fixation, the tissue was washed, and the pituitary was exposed from the ventral side by carefully removing the palate bone covering it. A single (1,1'-dioctadecyl-3,3,3',3'-tetramethylindocarbocyanine perchlorate) DiI crystal was then implanted into the pituitary tissue, and the preparation was incubated in 4% PFA in PBS for an additional 2 weeks in the dark at room temperature. Following the incubation, brains were dissected from the surrounding skull and imaged on a two-photon microscope.

### Chemical ablation of GnRH3 cells

Chemical ablation was performed on Tg(GnRH3:gal4ff; UAS:NTR-mCherry). Adult females (transgenic and nontransgenic) were crossed to males in individual spawning tanks over 7 days. Only females that spawned ( $n = 6$  per treatment) were chosen for the experiments. Eggs were collected and counted manually. Females were then treated overnight in 10  $\mu$ M metronidazole (in the dark) and allowed to recover in clean system water. One month after the treatment, the females were once more crossed to males, and spawning

attempts were repeated seven times over 7 days or until a successful spawn occurred. At the end of the experimental period, fish were sacrificed, and gonads and brains were collected for histology (gonads) and imaging (brains).

### MK-801 experiments

Tg(GnRH3:gal4ff; UAS:GCaMP6s) embryos were raised in E3 medium for 3 days and subsequently transferred to MK-801 solution (20, 50, and 200  $\mu$ M in E3). Larvae were incubated in the solutions for an additional 3 days at 28°C. Solutions were replaced daily. Fish were subjected to calcium imaging at day 3 (6 hours after the beginning of treatment) and at day 6. Subsequently, fish were fixed and immunostained using anti-GFP antibodies. Full Z-stacks of the GnRH3 circuit were obtained on a confocal microscope (Leica SP8), and cells were manually counted on images and sorted into categories (nasal, NFJ cluster, or brain).

### Morphological analysis

For extracting morphological parameters of GnRH3 neurons, we used immunostained Tg(GnRH3:RCaMP2) transgenic larvae at 4 to 7 dpf. Z-stacks were acquired using confocal imaging, and individual cell bodies were manually traced using ImageJ. Morphological parameters (roundness, circularity, and aspect ratio) were extracted using the same software. In total, we analyzed 52 nasal cells, 74 NFJ cells, and 47 brain cells from 10 fish.

### Statistical analysis

Statistical analysis was performed using Prism 8 software (Graph-Pad). Whiskers on bar plots represent means  $\pm$  SEM. Whiskers on individual value plots represent median  $\pm$  95% confidence interval. In violin plots, middle line represents median, whereas bottom and top lines represent lower and upper quartiles, respectively. Datasets were tested for equal variances (using Bartlett's test) and normality (using D'Agostino and Pearson's test). Dataset pairs that exhibited equal variances and normal distribution were compared using two-tailed Student's *t* test (for two sets) or one-way analysis of variance (ANOVA), followed by Tukey-Kramer test (for more than two sets). Datasets with different variances and/or non-Gaussian distributions were tested using two-tailed Mann-Whitney's test (for two sets) or Brown-Forsythe's one-way ANOVA, followed by Dunnett's T3 multiple comparisons test. Differences in the distribution pattern of neurons along the migration pathway were tested using Kolmogorov-Smirnov test. Pearson's  $\chi^2$  was used to test whether overexpression of kir2.1 significantly affected the frequency of GnRH cells within the three categories (nasal, NFJ, and brain). Significance was imparted at  $P < 0.05$  (n.s., nonsignificant; \* $P < 0.05$ ; \*\* $P < 0.01$ ; \*\*\* $P < 0.001$ ; \*\*\*\* $P < 0.0001$ ).

### SUPPLEMENTARY MATERIALS

Supplementary material for this article is available at <http://advances.sciencemag.org/cgi/content/full/7/8/eabc8475/DC1>

[View/request a protocol for this paper from Bio-protocol.](#)

### REFERENCES AND NOTES

- M. Schwanzel-Fukuda, D. W. Pfaff, Origin of luteinizing hormone-releasing hormone neurons. *Nature* **338**, 161–164 (1989).
- H.-J. Cho, Y. Shan, N. C. Whittington, S. Wray, Nasal placode development, GnRH neuronal migration and Kallmann syndrome. *Front. Cell Dev. Biol.* **7**, 121 (2019).
- A. E. Herbison, Control of puberty onset and fertility by gonadotropin-releasing hormone neurons. *Nat. Rev. Endocrinol.* **12**, 452–466 (2016).
- E. M. Mulrenin, J. W. Witkin, A.-J. Silverman, Embryonic development of the gonadotropin-releasing hormone (GnRH) system in the chick: A spatio-temporal analysis of GnRH neuronal generation, site of origin, and migration. *Endocrinology* **140**, 422–433 (1999).
- S. M. Fueshko, S. Key, S. Wray, GABA inhibits migration of luteinizing hormone-releasing hormone neurons in embryonic olfactory explants. *J. Neurosci.* **18**, 2560–2569 (1998).
- F. Casoni, S. A. Malone, M. Belle, F. Luzzati, F. Collier, C. Allet, E. Hrabovszky, S. Rasika, V. Prevot, A. Chédotal, P. Giacobini, Development of the neurons controlling fertility in humans: New insights from 3D imaging and transparent fetal brains. *Development* **143**, 3969–3981 (2016).
- A. Kitazawa, K. Kubo, K. Hayashi, Y. Matsunaga, K. Ishii, K. Nakajima, Hippocampal pyramidal neurons switch from a multipolar migration mode to a novel “climbing” migration mode during development. *J. Neurosci.* **34**, 1115–1126 (2014).
- C. Ohtaka-Maruyama, M. Okamoto, K. Endo, M. Oshima, N. Kaneko, K. Yura, H. Okado, T. Miyata, N. Maeda, Synaptic transmission from subplate neurons controls radial migration of neocortical neurons. *Science* **360**, 313–317 (2018).
- J. Altman, S. A. Bayer, Prolonged sojourn of developing pyramidal cells in the intermediate zone of the hippocampus and their settling in the stratum pyramidale. *J. Comp. Neurol.* **301**, 343–364 (1990).
- H. J. Luhmann, A. Fukuda, W. Kilb, Control of cortical neuronal migration by glutamate and GABA. *Front. Cell. Neurosci.* **9**, 4 (2015).
- H. Komuro, P. Rakic, Modulation of neuronal migration by NMDA receptors. *Science* **260**, 95–97 (1993).
- J. Q. Zheng, M. Poo, Calcium signaling in neuronal motility. *Annu. Rev. Cell Dev. Biol.* **23**, 375–404 (2007).
- H. Komuro, P. Rakic, Intracellular Ca<sup>2+</sup> fluctuations modulate the rate of neuronal migration. *Neuron* **17**, 275–285 (1996).
- B. I. Hutchins, U. Klente, S. Wray, Calcium release-dependent actin flow in the leading process mediates axophilic migration. *J. Neurosci.* **33**, 11361–11371 (2013).
- E.-L. Yap, M. E. Greenberg, Activity-regulated transcription: Bridging the gap between neural activity and behavior. *Neuron* **100**, 330–348 (2018).
- S. W. Flavell, M. E. Greenberg, Signaling mechanisms linking neuronal activity to gene expression and plasticity of the nervous system. *Annu. Rev. Neurosci.* **31**, 563–590 (2008).
- N. Hurni, M. Kolodziejczak, U. Tomasello, J. Badia, M. Jacobshagen, J. Prados, A. Dayer, Transient cell-intrinsic activity regulates the migration and laminar positioning of cortical projection neurons. *Cereb. Cortex* **27**, 3052–3063 (2017).
- Y. Bando, K. Irie, T. Shimomura, H. Umeshima, Y. Kushida, M. Kengaku, Y. Fujiyoshi, T. Hirano, Y. Tagawa, Control of spontaneous Ca<sup>2+</sup> transients is critical for neuronal maturation in the developing neocortex. *Cereb. Cortex* **26**, 106–117 (2016).
- R. Aguillon, J. Batut, A. Subramanian, R. Madelaine, P. Dufourcq, T. F. Schilling, P. Blader, Cell-type heterogeneity in the early zebrafish olfactory epithelium is generated from progenitors within preplacodal ectoderm. *eLife* **7**, e32041 (2018).
- E. Abraham, O. Palevitch, S. Ijiri, S. J. Du, Y. Gothilf, Y. Zohar, Early development of forebrain gonadotropin-releasing hormone (GnRH) neurons and the role of GnRH as an autocrine migration factor. *J. Neuroendocrinol.* **20**, 394–405 (2008).
- M. Golan, E. Zelinger, Y. Zohar, B. Levavi-Sivan, Architecture of GnRH-gonadotropin-vasculature reveals a dual mode of gonadotropin regulation in fish. *Endocrinology* **156**, 4163–4173 (2015).
- E. Abraham, O. Palevitch, Y. Gothilf, Y. Zohar, Targeted gonadotropin-releasing hormone-3 neuron ablation in zebrafish: Effects on neurogenesis, neuronal migration, and reproduction. *Endocrinology* **151**, 332–340 (2010).
- Y. Shan, H. Saadi, S. Wray, Heterogeneous origin of gonadotropin releasing hormone-1 neurons in mouse embryos detected by islet-1/2 expression. *Front. Cell Dev. Biol.* **8**, 35 (2020).
- Y. Zhao, M.-C. A. Lin, M. Farajzadeh, N. L. Wayne, Early development of the gonadotropin-releasing hormone neuronal network in transgenic zebrafish. *Front. Endocrinol. (Lausanne)* **4**, 107 (2013).
- K. E. Whitlock, C. D. Wolf, M. L. Boyce, Gonadotropin-releasing hormone (GnRH) cells arise from cranial neural crest and adenohipophyseal regions of the neural plate in the zebrafish, *Danio rerio*. *Dev. Biol.* **257**, 140–152 (2003).
- Y. Liu, H. Tang, R. Xie, S. Li, X. Liu, H. Lin, Y. Zhang, C. H. K. Cheng, Genetic evidence for multifactorial control of the reproductive axis in zebrafish. *Endocrinology* **158**, 604–611 (2017).
- O. S. Spicer, T.-T. Wong, N. Zmora, Y. Zohar, Targeted mutagenesis of the hypophysiotropic GnRH3 in zebrafish (*Danio rerio*) reveals no effects on reproductive performance. *PLOS ONE* **11**, e0158141 (2016).
- M. Marvel, O. S. Spicer, T. T. Wong, N. Zmora, Y. Zohar, Knockout of the GnRH genes in zebrafish: Effects on reproduction and potential compensation by reproductive and feeding-related neuropeptides. *Biol. Reprod.* **99**, 565–577 (2018).
- V. L. Trudeau, Facing the challenges of neuropeptide gene knockouts: Why do they not inhibit reproduction in adult teleost fish? *Front. Neurosci.* **12**, 302 (2018).
- R. Ando, H. Hama, M. Yamamoto-Hino, H. Mizuno, A. Miyawaki, An optical marker based on the UV-induced green-to-red photoconversion of a fluorescent protein. *Proc. Natl. Acad. Sci. U.S.A.* **99**, 12651–12656 (2002).

31. S. Constantin, C. Jasoni, N. Romanò, K. Lee, A. E. Herbison, Understanding calcium homeostasis in postnatal gonadotropin-releasing hormone neurons using cell-specific Pericam transgenics. *Cell Calcium* **51**, 267–276 (2012).
32. C. M. Niell, M. P. Meyer, S. J. Smith, In vivo imaging of synapse formation on a growing dendritic arbor. *Nat. Neurosci.* **7**, 254–260 (2004).
33. Y. Yoshihara, T. Mizuno, M. Nakahira, M. Kawasaki, Y. Watanabe, H. Kagamiyama, K. Jishage, O. Ueda, H. Suzuki, K. Tabuchi, K. Sawamoto, H. Okano, T. Noda, K. Mori, A genetic approach to visualization of multisynaptic neural pathways using plant lectin transgene. *Neuron* **22**, 33–41 (1999).
34. S. X. Simonian, A. E. Herbison, Differing, spatially restricted roles of ionotropic glutamate receptors in regulating the migration of GnRH neurons during embryogenesis. *J. Neurosci.* **21**, 934–943 (2001).
35. R. J. Clarke, J. W. Johnson, NMDA receptor NR2 subunit dependence of the slow component of magnesium unblock. *J. Neurosci.* **26**, 5825–5834 (2006).
36. A. Momiya, D. Feldmeyer, S. G. Cull-Candy, Identification of a native low-conductance NMDA channel with reduced sensitivity to Mg<sup>2+</sup> in rat central neurones. *J. Physiol.* **494**, 479–492 (1996).
37. J. G. Orlandi, J. Soriano, E. Alvarez-Lacalle, S. Teller, J. Casademunt, Noise focusing and the emergence of coherent activity in neuronal cultures. *Nat. Phys.* **9**, 582–590 (2013).
38. Y. Penn, M. Segal, E. Moses, Network synchronization in hippocampal neurons. *Proc. Natl. Acad. Sci. U.S.A.* **113**, 3341–3346 (2016).
39. E. Cohen, M. Ivenshitz, V. Amor-Barouk, V. Greenberger, M. Segal, Determinants of spontaneous activity in networks of cultured hippocampus. *Brain Res.* **1235**, 21–30 (2008).
40. H. Yamamoto, S. Moriya, K. Ide, T. Hayakawa, H. Akima, S. Sato, S. Kubota, T. Tani, M. Niwano, S. Teller, J. Soriano, A. Hirano-Iwata, Impact of modular organization on dynamical richness in cortical networks. *Sci. Adv.* **4**, eaau4914 (2018).
41. S. Teller, E. Estévez-Priego, C. Granell, D. Tornero, J. Andilla, O. E. Olarte, P. Loza-Alvarez, A. Arenas, J. Soriano, Spontaneous functional recovery after focal damage in neuronal cultures. *eNeuro* **7**, ENEURO.0254-19.2019 (2020).
42. A. Majdandzic, B. Podobnik, S. V. Buldyrev, D. Y. Kenett, S. Havlin, H. Eugene Stanley, Spontaneous recovery in dynamical networks. *Nat. Phys.* **10**, 34–38 (2014).
43. D. C. Johns, R. Marx, R. E. Mains, B. O'Rourke, E. Marbán, Inducible genetic suppression of neuronal excitability. *J. Neurosci.* **19**, 1691–1697 (1999).
44. S. Wray, Development of gonadotropin-releasing hormone-1 neurons. *Front. Neuroendocrinol.* **23**, 292–316 (2002).
45. S. Wray, From nose to brain: Development of gonadotrophin-releasing hormone-1 neurones. *J. Neuroendocrinol.* **22**, 743–753 (2010).
46. Y. Chen, Y. Wang, Z. Modrusan, M. Sheng, J. S. Kaminker, Regulation of neuronal gene expression and survival by basal NMDA receptor activity: A role for histone deacetylase 4. *J. Neurosci.* **34**, 15327–15339 (2014).
47. A. Karpova, M. Mikhaylova, S. Bera, J. Bär, P. P. Reddy, T. Behnisch, V. Rankovic, C. Spilker, P. Bethge, J. Sahin, R. Kaushik, W. Zschratler, T. Kähne, M. Naumann, E. D. Gundelfinger, M. R. Kreutz, Encoding and transducing the synaptic or extrasynaptic origin of NMDA receptor signals to the nucleus. *Cell* **152**, 1119–1133 (2013).
48. K. Miura, J. S. Acierio Jr., S. B. Seminara, Characterization of the human nasal embryonic LHRH factor gene, NELF, and a mutation screening among 65 patients with idiopathic hypogonadotropic hypogonadism (IHH). *J. Hum. Genet.* **49**, 265–268 (2004).
49. N. Pitteloud, R. Quinton, S. Pearce, T. Raivio, J. Acierio, A. Dwyer, L. Plummer, V. Hughes, S. Seminara, Y.-Z. Cheng, W.-P. Li, G. Maccoll, A. V. Eliseenkova, S. K. Olsen, O. A. Ibrahim, F. J. Hayes, P. Boepple, J. E. Hall, P. Bouloux, M. Mohammadi, W. Crowley, Digenic mutations account for variable phenotypes in idiopathic hypogonadotropic hypogonadism. *J. Clin. Invest.* **117**, 457–463 (2007).
50. J. P. Moore Jr., E. Shang, S. Wray, In situ GABAergic modulation of synchronous gonadotropin releasing hormone-1 neuronal activity. *J. Neurosci.* **22**, 8932–8941 (2002).
51. G. Martínez de la Escalera, A. L. Choi, R. I. Weiner, Generation and synchronization of gonadotropin-releasing hormone (GnRH) pulses: Intrinsic properties of the GT1-1 GnRH neuronal cell line. *Proc. Natl. Acad. Sci. U.S.A.* **89**, 1852–1855 (1992).
52. J.-B. Manent, M. Demarque, I. Jorquera, C. Pellegrino, Y. Ben-Ari, L. Aniksztejn, A. Represa, A noncanonical release of GABA and glutamate modulates neuronal migration. *J. Neurosci.* **25**, 4755–4765 (2005).
53. A. E. Herbison, R. Porteous, J.-R. Pape, J. M. Mora, P. R. Hurst, Gonadotropin-releasing hormone neuron requirements for puberty, ovulation, and fertility. *Endocrinology* **149**, 597–604 (2008).
54. F. Birey, J. Andersen, C. D. Makinson, S. Islam, W. Wei, N. Huber, H. C. Fan, K. R. C. Metzler, G. Panagiotakos, N. Thom, N. A. O'Rourke, L. M. Steinmetz, J. A. Bernstein, J. Hallmayer, J. R. Huguenard, S. P. Pasca, Assembly of functionally integrated human forebrain spheroids. *Nature* **545**, 54–59 (2017).
55. M. Golan, J. Biran, B. Levavi-Sivan, A novel model for development, organization, and function of gonadotropes in fish pituitary. *Front. Endocrinol. (Lausanne)* **5**, 182 (2014).
56. J. Boulanger-Weill, V. Candat, A. Jouary, S. A. Romano, V. Pérez-Schuster, G. Sumbre, Functional interactions between newborn and mature neurons leading to integration into established neuronal circuits. *Curr. Biol.* **27**, 1707–1720.e5 (2017).
57. M. Takeuchi, K. Matsuda, S. Yamaguchi, K. Asakawa, N. Miyasaka, P. Lal, Y. Yoshihara, A. Koga, K. Kawakami, T. Shimizu, M. Hibi, Establishment of Gal4 transgenic zebrafish lines for analysis of development of cerebellar neural circuitry. *Dev. Biol.* **397**, 1–17 (2015).
58. A. Filosa, A. J. Barker, M. Dal Maschio, H. Baier, Feeding state modulates behavioral choice and processing of prey stimuli in the zebrafish tectum. *Neuron* **90**, 596–608 (2016).
59. M. Inoue, A. Takeuchi, S. Horigane, M. Ohkura, K. Gengyo-Ando, H. Fujii, S. Kamijo, S. Takemoto-Kimura, M. Kano, J. Nakai, K. Kitamura, H. Bito, Rational design of a high-affinity, fast, red calcium indicator R-CaMP2. *Nat. Methods* **12**, 64–70 (2015).
60. J. R. Sternberg, K. E. Severi, K. Fidelin, J. Gomez, H. Ihara, Y. Alcheikh, J. M. Hubbard, K. Kawakami, M. Suster, C. Wyart, Optimization of a neurotoxin to investigate the contribution of excitatory interneurons to speed modulation in vivo. *Curr. Biol.* **26**, 2319–2328 (2016).
61. E. J. Horstick, D. C. Jordan, S. A. Bergeron, K. M. Tabor, M. Serpe, B. Feldman, H. A. Burgess, Increased functional protein expression using nucleotide sequence features enriched in highly expressed genes in zebrafish. *Nucleic Acids Res.* **43**, e48 (2015).
62. S. Mahabir, D. Chatterjee, K. Misquitta, D. Chatterjee, R. Gerlai, Lasting changes induced by mild alcohol exposure during embryonic development in BDNF, NCAM and synaptophysin-positive neurons quantified in adult zebrafish. *Eur. J. Neurosci.* **47**, 1457–1473 (2018).
63. S. A. Romano, V. Pérez-Schuster, A. Jouary, J. Boulanger-Weill, A. Candeo, T. Pietri, G. Sumbre, An integrated calcium imaging processing toolbox for the analysis of neuronal population dynamics. *PLoS Comput. Biol.* **13**, e1005526 (2017).
64. T. W. Chen, T. J. Wardill, Y. Sun, S. R. Pulver, S. L. Renninger, A. Baohan, E. R. Schreiter, R. A. Kerr, M. B. Orger, V. Jayaraman, L. L. Looger, K. Svoboda, D. S. Kim, Ultrasensitive fluorescent proteins for imaging neuronal activity. *Nature* **499**, 295–300 (2013).
65. N. Romanò, S. H. Yip, D. J. Hodson, A. Guillo, S. Parnaudeau, S. Kirk, F. Tronche, X. Bonnefont, P. Le Tissier, S. J. Bunn, D. R. Grattan, P. Mollard, A. O. Martin, Plasticity of hypothalamic dopamine neurons during lactation results in dissociation of electrical activity and release. *J. Neurosci.* **33**, 4424–4433 (2013).
66. C. Thisse, B. Thisse, High-resolution in situ hybridization to whole-mount zebrafish embryos. *Nat. Protoc.* **3**, 59–69 (2008).
67. E. A. Susaki, K. Tainaka, D. Perrin, F. Kishino, T. Tawara, T. M. Watanabe, C. Yokoyama, H. Onoe, M. Eguchi, S. Yamaguchi, T. Abe, H. Kiyonari, Y. Shimizu, A. Miyawaki, H. Yokota, H. R. Ueda, Whole-brain imaging with single-cell resolution using chemical cocktails and computational analysis. *Cell* **157**, 726–739 (2014).

**Acknowledgments:** We would like to thank F. Ango (IGF, Montpellier, France), D. Hodson (University of Birmingham, UK), and M. Gutnick (Hebrew University of Jerusalem, Israel) for the critical reading of the manuscript and comments. We thank M. Mangoni (IGF, Montpellier) for providing the fish rearing system. C. Joplion provided invaluable assistance and support in setting up and maintaining our fish colony and shared zebrafish-related resources. G. Sumbre (IBENS, Paris) allowed us to use his two-photon microscope for the multicolor 2P imaging. G. Levkowitz and P. Rajamannar (Weizmann Institute of Science, Israel) helped with additional calcium imaging and provided support during the revision process. M. Asari (IGF, Montpellier) generated the graphical summary model (Fig. 6F). C. Lafont (IPAM-BioCampus, Montpellier) assisted with multiple imaging-related issues and final figure preparation. IPAM-BioCampus Montpellier platform is quality-certified ISO 9001-2015. **Funding:** This research was funded by the H2020 Marie S. Curie Fellowship Program H2020-MSCA-IF-2014 grant number 656763-GTHREG (to M.G.), ANR-CONACyT 273513, Estancia Sabática apoyada con el Programa PASPADA-DGAPA UNAM (to T.F.-C.), Agence Nationale de la Recherche (ANR-15-CE14-0012 and ANR-18-CE14-0017) (to P.M.), Leducq Foundation ERPT grant (to P.M. and A.F.), FranceBioimaging ANR-10-INSB-04 “Investments for the Future” (to P.M.), Agence Nationale de la Recherche (ANR-18-CE92-0010-01) (to A.O.M.), and the India-Israel ARO Postdoctoral Fellowship Program (to D.S.G.). **Author contributions:** M.G. and P.M. conceived the project and designed the experiments. M.G., J.B.-W., A.P., T.F.-C., A.F., D.S.G., and A.O.M. performed the experiments. J.B.-W. and P.F. designed custom-made software. M.G., J.B.-W., P.F., and A.O.M. analyzed experimental data. L.H.-C. generated the Tg(GnRH3:ChR2-YFP) transgenic line. M.G. and P.M. wrote the manuscript with input from all other co-authors. **Competing interests:** The authors declare that they have no competing interests. **Data and materials availability:** All data needed to evaluate the conclusions in the paper are present in the paper and/or the Supplementary Materials. Additional data related to this paper may be requested from the authors.

Submitted 19 May 2020

Accepted 6 January 2021

Published 19 February 2021

10.1126/sciadv.abc8475

**Citation:** M. Golan, J. Boulanger-Weill, A. Pinot, P. Fontanaud, A. Faucherre, D. S. Gajbhiye, L. Hollander-Cohen, T. Fiordelisio-Coll, A. O. Martin, P. Mollard, Synaptic communication mediates the assembly of a self-organizing circuit that controls reproduction. *Sci. Adv.* **7**, eabc8475 (2021).



## Synaptic communication mediates the assembly of a self-organizing circuit that controls reproduction

M. Golan, J. Boulanger-Weill, A. Pinot, P. Fontanaud, A. Faucherre, D. S. Gajbhiye, L. Hollander-Cohen, T. Fiordelisio-Coll, A. O. Martin and P. Mollard

*Sci Adv* 7 (8), eabc8475.  
DOI: 10.1126/sciadv.abc8475

### ARTICLE TOOLS

<http://advances.sciencemag.org/content/7/8/eabc8475>

### SUPPLEMENTARY MATERIALS

<http://advances.sciencemag.org/content/suppl/2021/02/12/7.8.eabc8475.DC1>

### REFERENCES

This article cites 67 articles, 17 of which you can access for free  
<http://advances.sciencemag.org/content/7/8/eabc8475#BIBL>

### PERMISSIONS

<http://www.sciencemag.org/help/reprints-and-permissions>

Use of this article is subject to the [Terms of Service](#)

---

*Science Advances* (ISSN 2375-2548) is published by the American Association for the Advancement of Science, 1200 New York Avenue NW, Washington, DC 20005. The title *Science Advances* is a registered trademark of AAAS.

Copyright © 2021 The Authors, some rights reserved; exclusive licensee American Association for the Advancement of Science. No claim to original U.S. Government Works. Distributed under a Creative Commons Attribution NonCommercial License 4.0 (CC BY-NC).